This CVPR paper is the Open Access version, provided by the Computer Vision Foundation.
Except for this watermark, it is identical to the accepted version;
the final published version of the proceedings is available on IEEE Xplore.

BHCAST: Unlocking Black Hole Plasma Dynamics from a Single Blurry Image with Long-Term Forecasting

Renbo Tu[1,2] Ali SaraerToosi[1,2] Nicholas S. Conroy[3] Gennady Pekhimenko[1,2,4] Aviad Levis[1,2]
[1]*University of Toronto* [2] *Vector Institute* [3] *University of Illinois at Urbana-Champaign* [4] *NVIDIA*

Abstract

The Event Horizon Telescope (EHT) delivered the first image of a black hole by capturing the light from its surrounding accretion flow, revealing structure but not dynamics. Simulations of black hole accretion dynamics are essential for interpreting EHT images but costly to generate and impractical for inference. Motivated by this bottleneck, BHCAST *presents a framework for forecasting black hole plasma dynamics from a single, blurry snapshot, such as those captured by the EHT. At its core,* BHCAST *is a neural model that transforms a static image into forecasted future frames, revealing the underlying dynamics hidden within one snapshot. With a multi-scale pyramid loss, we demonstrate how autoregressive forecasting can simultaneously super-resolve and evolve a blurry frame into a coherent, high-resolution movie that remains stable over long time horizons. From forecasted dynamics, we can then extract interpretable spatio-temporal features, such as pattern speed (rotation rate) and pitch angle. Finally,* BHCAST *uses gradient-boosting trees to recover black hole properties from these plasma features, including the spin and viewing inclination angle. The separation between forecasting and inference provides modular flexibility, interpretability, and robust uncertainty quantification. We demonstrate the effectiveness of* BHCAST *on simulations of two distinct black hole accretion systems, Sagittarius A* and M87*, by testing on simulated frames blurred to EHT resolution and real EHT images of M87*. Ultimately, our methodology establishes a scalable paradigm for solving inverse problems, demonstrating the potential of learned dynamics to unlock insights from resolution-limited scientific data.*

1. Introduction

The Event Horizon Telescope (EHT) has captured the first images of M87* and Sagittarius A* (Sgr A*) black holes, a landmark in both astrophysics and imaging science, achieving the highest angular resolution ever recorded in astronomy [15, 16]. To reach this resolution, data from worldwide radio telescopes are combined using Very Long Baseline Interferometry (VLBI). The result is the first visual evidence of a black hole event horizon. Nonetheless, these static images provide limited insight into the complex plasma dynamics that power black hole accretion. Capturing and understanding their temporal evolution is key to interpreting EHT data and probing the underlying plasma dynamics [9].

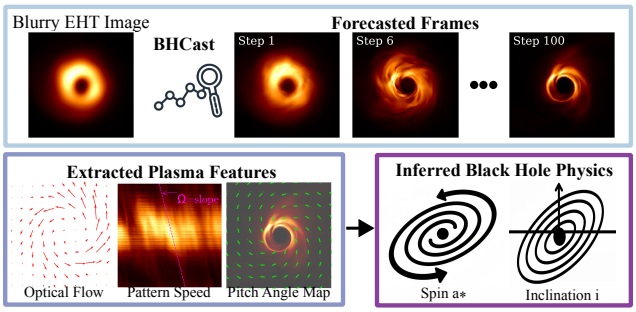


Figure 1. **From a Single Blurry Frame to Black-Hole Dynamics.** A single blurry image, reconstructed from Event Horizon Telescope measurements, is used to forecast a dynamic sequence of high-resolution frames. From this forecasted movie, features of accretion disk plasma can be extracted to infer the black hole's physical properties. This sequential framework—forecasting, feature extraction, and parameter estimation—is robust, versatile, and fully interpretable, providing a new pathway for analyzing horizon-scale dynamics.

To bridge the gap between static images and dynamics, astrophysicists are developing extensive libraries of time-dependent General Relativistic Magnetohydrodynamics (GRMHD) simulations [42, 45] which involve solving nonlinear equations of general relativity coupled to multi-scale magneto-hydrodynamics equations for magnetized fluids [14]. These highly-complex simulations, for the most part, show remarkable consistency with observation data [1, 2, 63]. Inferring black hole properties from such simulations relies on scanning a massive library of GRMHD simulations to find the best match to observations. This process is computationally prohibitive, as a single simulation can take weeks on a supercomputer, making exploration of large or fine-grained parameter spaces infeasible [14].

This computational bottleneck motivates our work (Fig. 1), which builds on recent advances in physics-informed deep learning [32, 46]. We replace the expensive

forward GRMHD simulation with a lightweight neural surrogate, which is highly efficient on modern GPUs. Neural surrogate models for fluid dynamics have gained significant traction in recent years, but extending them to black hole plasmas from reconstructed (rather than simulated) EHT images introduces a unique set of challenges [7, 35, 36, 46]. First, EHT images are fundamentally resolution-limited by the telescope's $\sim 20\mu as$ (micro-arcsecond) beam, creating an ill-posed inverse problem [1]. Recovering the lost high-frequency information, a super-resolution task, is essential to reveal the subtle cues of plasma dynamics encoded in these images. Second, key indicators of black hole dynamics require stable forecasts over long temporal horizons of 300 GMc^{-3}[1] to be measured accurately [9]. Existing research focuses on single-step predictions, while autoregressive forecasts of long-term dynamics remain a major challenge due to rapid error accumulation [35, 36, 46].

In this paper, we introduce BHCAST, a long-term forecasting framework designed to produce high-fidelity, super-resolved simulation dynamics from a single, blurry black hole image. Our framework overcomes the instability of autoregressive prediction by incorporating a multi-scale pyramid loss during training. We demonstrate this super-resolution effect and the stability of our predictions in simulations (Fig. 2). Using the forecasted frames, we extract key plasma features that characterize the dynamic and geometric properties of the black hole accretion flow. As an application of BHCAST for inverse problems, we train an XGBoost model to predict black hole parameters from the computed plasma features. Note that our framework provides interpretable inference of plasma and black hole parameters, as recovered parameters can be traced back to visual cues in the forecasted frames. Furthermore, our modular design allows for future improvements across different stages of the BHCAST pipeline.

We evaluate the framework in forecasting, feature extraction, and parameter inference. For long-term forecasting, we demonstrate that BHCAST produces super-resolved and temporally stable predictions, outperforming both end-to-end deep learning and traditional computer vision baselines. For plasma feature extraction and black hole parameter inference, BHCAST is more robust to noise compared to direct inference with a black-box supervised baseline.

In summary, we make the following core contributions:

1. We recast a challenging, ill-posed astrophysical imaging task as a forecasting+inference problem, enabling the use of efficient neural surrogates for rapid black hole characterization. Our reformulation provides a useful roadmap for future works in scientific imaging.

[1]For gravitational constant G, black hole mass M, and speed of light c, GMc^{-3} is the characteristic dynamical timescale near the event horizon which depends on the black hole mass: ∼20 seconds for Sgr A* and ∼9 hours for M87*.

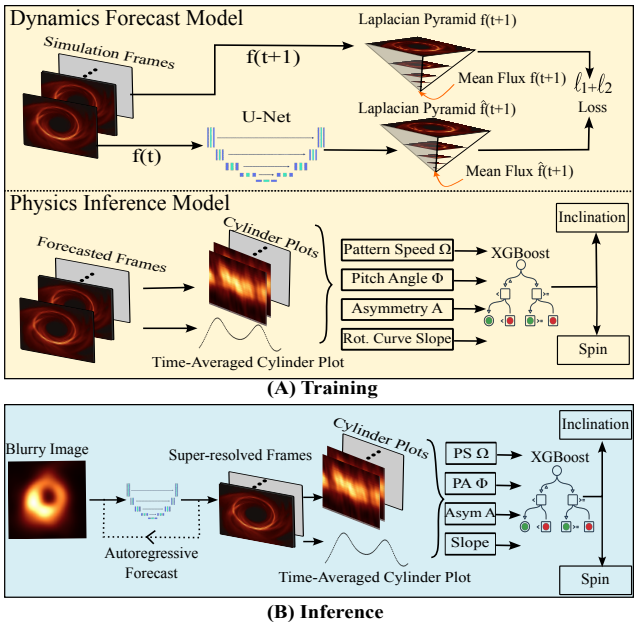


Figure 2. **Training and inference pipelines of BHCAST.** We train the dynamics forecast model (U-Net) to predict the next frame and the physics inference model (XGBoost) to estimate black hole parameters. During inference, we autoregressively forecast with the U-Net to produce cylinder plots to extract plasma features, which are inputs to XGBoost for physics inference.

2. Leveraging a physics-informed multi-scale loss, our dynamics surrogate model super-resolves blurry input images and forecasts stable evolution for up to 100 steps, (500 GMc^{-3} or 10,000 seconds on Sgr A*), sufficiently long for precise physical measurements. We demonstrate forecasting on real EHT images of M87*
3. BHCAST produces high-fidelity forecasts with accurate dynamic and geometric plasma features. On four features, the forecast error is comparable with a baseline of four ResNet models trained separately on each feature.
4. For parameter inference, BHCAST estimates black hole spin and inclination angle better than ResNet, demonstrating better robustness to input noise compared to direct inference.

2. Related Works

Multi-Scale and Self-Similarity in Vision Multi-scale representations are foundational in computer vision, from classical pyramid decompositions [6] to coarse-to-fine inference and internal image statistics. Natural images exhibit strong cross-scale self-similarity, a principle exploited in seminal works on super-resolution and deblurring [22, 33, 40, 67]. These methods show that fine-scale structure can often be reconstructed from recurring patterns already present within a single image. Although developed for natural images, this multi-scale and self-similar perspective

aligns well with the fractal, turbulent structure of black hole plasmas, motivating our use of a hierarchical loss to recover high-frequency detail from sparse, resolution-limited data.

Modeling Dynamics Neural surrogates for dynamical systems typically follow one of two strategies: next-frame prediction or full-sequence generation. Data-hungry diffusion-based approaches for GRMHD data fall into the latter category, generating entire video sequences in a single pass but requiring the forecast horizon to be fixed a priori [65]. Next-frame prediction is more versatile, as a model can be rolled out autoregressively for arbitrarily long horizons, but this flexibility comes at the cost of compounding errors and potential instability during rollout [52]. While Fourier Neural Operators are strong in learning PDE-driven dynamics, they are better suited for systems with global behaviors rather than black holes with local turbulence [35, 36]. For these reasons, BHCAST adopts a data-efficient U-Net for next-frame prediction and explicitly addresses long-horizon stability to recover plasma evolution.

Black Hole Parameter Estimation Inferring physical parameters from EHT observations typically follows one of two approaches: direct inference from EHT visibilities in the frequency domain, or image-based inference in the pixel domain. Recent visibility-domain methods use adaptive Bayesian inference, but their non-parallelizable MCMC loops create a major computational bottleneck, with individual runs taking up to 20 CPU hours [64]. To avoid this cost, feed-forward machine learning approaches based on visibility data products have been used for classification [57], however, this approach is limited to inference of simple physical models. Conversely, image-based inference using supervised learning, explored by Deep Horizon and its extensions, offers a faster alternative [19, 58]. The primary drawback of these "black-box" approaches is their failure to capture black hole dynamics, limiting the physical interpretability of their predictions. Other methods, such as those based on random fields, can infer from both visibilities and images, but they have thus far been limited to a small, fixed set of parameters [34].

3. Background

Black Hole EHT-Imaging The EHT achieves an unprecedented angular resolution of $\sim$ 20 μas by combining millimeter and sub-millimeter radio telescope observations across the globe [16]. Despite the resolution, reconstructed images remain inherently uncertain due to various factors including interstellar scattering, sparse coverage, and source variability [16, 30, 31, 55]. Together, these effects imply that EHT images can be modeled as a convolution of the intrinsic black hole emission structure with both astrophysical and instrumental blurring. Despite these challenges, our hypothesis is that the EHT images contain rich dynamical information encoded in the blurry image morphology. Two quantities proposed to characterize black hole dynamics are: (i) the **pitch angle**, which is the angle between a spiral pattern and the local azimuthal direction [3, 47], and (ii) the **pattern speed**, which is the angular rate at which a coherent structure (like a spiral arm or brightness pattern) rotates [9].

GRMHD Simulations A key challenge in analyzing black hole EHT images is the highly variable environment of the accretion flow, and the plasma around a black hole is analytically intractable. GRMHD simulations therefore serve as the current gold standard for self-consistently modeling black hole accretion flows [44]. The resulting 3D plasma states are rendered into 2D image-plane intensities by general-relativistic ray tracing, through integration of the radiative transfer equations [42]. Two key physical parameters that characterize the morphology and dynamics of the flow in the image plane are: first, the viewing inclination angle i, which sets the angle between the observer's line of sight and the angular momentum vector of the accretion disk; and second, the dimensionless black hole spin a_*, which affects both the emission morphology and the photon trajectories near the event horizon that shape the observed image. The movies have a time resolution of 5 GMc^{-3} and an angular resolution of 0.5 μas. More information is available in Appendix C [11, 56, 63].

Dynamical Systems Attractor and Dissipativity Many complex physical processes, including turbulent flows, can be described as dissipative dynamical systems [41]. A key property of such systems is that their long-term behavior collapses from a high-dimensional state space onto a lower-dimensional, bounded set known as a global attractor. This attractor represents the stable, invariant manifold containing all physically-plausible states of the system's dynamics [36]. Crucially, these systems possess a *basin of attraction*: trajectories originating from a larger set of initial conditions, even *off-manifold* states such as a blurry image, are rapidly "pulled" onto the attractor by the system's evolution [12, 13]. This dissipative "pull" is the theoretical basis for our model's super-resolution. Furthermore, once a trajectory is on this stable manifold, it remains there, which is what enables stable, long-horizon forecasting.

4. The BHCAST Framework

In this section, we introduce BHCAST as a framework that first forecasts dynamics, then extracts plasma features, and finally infers black hole parameters.

4.1. GRMHD Dynamics Forecast Model

The core of BHCAST is a dynamics forecast model whose goal is to predict the next state (or frame) of the black hole accretion flow from the current state. This is equivalent to

learning a mapping $f(x_t) \mapsto x_{t+1}$, where $x_t \in X$ represents all possible states of the flow. While many neural architectures for spatio-temporal forecasting exist, including powerful models such as transformers and neural operators, we select the U-Net architecture for its data-efficiency and inherent convolutional inductive bias for capturing local turbulent fluctuations in GRMHDs [35, 49, 59].

A key requirement of the dynamics model is to perform stable, autoregressive prediction for N iterations $(f^N(x_0))$ from a blurry initial state x_0. The model should simultaneously super-resolve this initial state and maintain stable, physically-plausible dynamics over a long time horizon. In dynamical systems terms, long-term predictions are expected to approach and remain within the global attractor A [36]. However, a vanilla U-Net trained on the default ℓ_2 loss rapidly accumulates error and diverges. As a preliminary step, we log-normalize the states to compress the dynamic range for numerical stability. More crucially, we introduce a multi-scale loss structure for training.

Multi-Scale Laplacian Pyramid Loss Standard pixel-wise losses such as ℓ_2 treat all spatial frequencies equally, which makes them poorly suited for preserving the holistic disk structure and fine-scale spiral features present in GRMHD frames. To encourage consistency across frequencies, we adopt a Laplacian pyramid loss that applies supervision at multiple spatial scales. Such multi-scale objectives have proven effective in stabilizing training and preserving structure in vision tasks [21].

Given M levels and downsample (average pooling), bilinear upsample operations, for level $k \in \{0, \dots M\}$,

$$\begin{aligned} Lap_k(I) &= G_k(I) - \text{Upscale}(G_{k+1}(I)) \\ G_k(I) &= \text{Downscale}(G_{k-1}(I)), G_0(I) = I \end{aligned} \tag{1}$$

A standard Laplacian pyramid on simulation frames has 7 layers, i.e. $k \in \{0, \dots 6\}$. Here, we make two key modifications: first, to save computation, we use a subset of the pyramid levels $k \in \{0, 1, 2, 6\}$ to include both the finest details $(k = 0)$ and intermediate-scale information $(k = 1, 2)$. However, computing the coarsest, single-pixel level $Lap_6 = G_6$ requires the previous level of the Gaussian pyramid, G_5. We make the second modification by replacing the coarsest level information Lap_6 with the mean flux, $\Phi(I)$, such that it can be computed independent of other levels. For an image with dimensions H, W,

$$Lap_6(I) \coloneqq \Phi(I) = \frac{1}{HW} \sum_{i=1}^{H} \sum_{j=1}^{W} I(i, j) \tag{2}$$

The mean flux, $\Phi(I)$, represents the spatially-integrated intensity of a single frame. A time-series of mean flux values construct the light curve, a crucial observable in many astrophysics topics beyond black holes, such as exoplanets and supernovae [24, 50, 62]. For black holes, the mean flux's relationship to the light curve makes it an important observable that constrains the entire energy output of the system. Thus, it is a physical constraint that complements the spatial structure encoded in other levels.

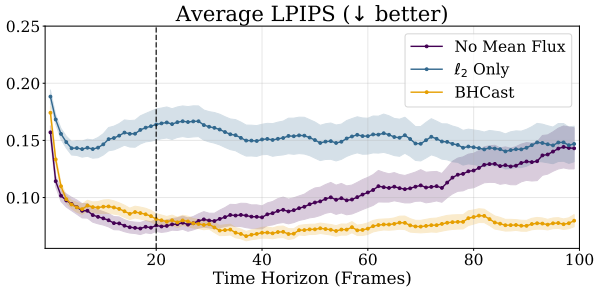


Figure 3. **Loss ablation study.** LPIPS across three losses: ℓ_2 only, multi-scale without mean-flux, and the full BHCAST loss. ℓ_2-only performs poorly at all times, while the multi-scale variant works briefly but becomes unstable. The full loss, combining multi-scale and mean-flux terms, yields stable long-term forecasts.

In summary, we construct the Laplacian pyramid for both prediction and ground truth to compute the loss term as a weighted sum of losses for each level:

$$\mathcal{L}_{total} = \sum \mathcal{L}_{Lap_0} + \frac{1}{2}\mathcal{L}_{Lap_1} + \frac{1}{4}\mathcal{L}_{Lap_2} + \frac{1}{8}\mathcal{L}_{\Phi} \tag{3}$$

The weights follow a heuristic scale factor and were not hand-tuned [6]. At each scale, the loss term combines ℓ_1 and ℓ_2 with equal weight to balance the outlier robustness of ℓ_1 and ease of optimization of ℓ_2.

To evaluate the fidelity of the restored details, we use the Learned Perceptual Image Patch Similarity (LPIPS, lower is better) metric, ensuring that recovered fine-grained structure reflects meaningful physical variability rather than noise [66]. LPIPS measures perceptual similarity beyond pixel-wise metrics like PSNR or SSIM. We perform an ablation study on the dynamics model's training loss. We train two additional dynamics models: (i) using only ℓ_2 and (ii) only Laplacian pyramid without the mean flux component. Fig. 3 shows these variants fail in long-term stable forecasting. The multi-scale, no-mean-flux model is only stable for the first 20 forecasts. This confirms the importance of mean flux regularization for long-term forecasting.

4.2. Extracting Plasma Features from Forecast

Following the autoregressive generation, BHCAST extracts plasma features from the forecasted frames using **cylinder plots**, which capture the dynamical and geometric properties of the accretion flow [9]. A cylinder plot $T(\theta, t)$ is a 2D function parameterized by position angle θ and time t, computed by sampling image intensities along a ring. The ring radius $\sqrt{27}\ GMc^{-2}D^{-1}$ [2] is chosen as it approximately

[2] D denotes distance to the black hole

corresponds to the critical impact parameter for Sgr A*, which defines the visible edge of the black hole shadow. Beyond the primary radius, we evaluate additional cylinder plots at multiple radii, enabling extraction of four quantitative features: two dynamical, (i) pattern speed and (ii) rotation curve slope, and two geometric, (iii) pitch angle and (iv) asymmetry [4, 9, 10, 47]. The following paragraphs introduce and define each of these features.

(i) Dynamics: Pattern Speed Ω_p The pattern speed, a measure of the apparent angular rotation rate defined through ratios of azimuthal image moments, serves as a statistical descriptor of how the overall structure rotates. Visually, pattern speed is the slope of the brightest feature on a normalized cylinder plot. Ω_p depends strongly on inclination angle, a key property of interest [9].

(ii) Dynamics: Rotation Curve Slope Recently, Conroy et al. found that rotation rates measured at different distances from the center of the dominant Sgr A* ring exhibit a *rotation curve*. Rotation speeds are faster closer to the black hole event horizon. The rate of change of the rotation speed at different angular radii, the *rotation curve slope*, varies with the black hole's spin parameter [10].

(iii) Geometry: Pitch Angle Φ This quantifies the geometry of coherent spiral structures in the flow by measuring how tightly wound the emission arms are around the black hole shadow [47]. It is estimated by comparing the azimuthal structure at neighboring radii in the cylinder plot and identifying the relative angular shift between them. Computationally, this is done by cross correlating two cylinder plots measured at r_{ring} and $r_{ring} + \delta_r$ [3]. Pitch angle is correlated with the inclination angle [9, 47].

(iv) Geometry: Asymmetry Asymmetry is the amplitude of the sinusoidal function fitted to the time-averaged cylinder plot. It measures the difference in brightness between the bright side of the ring and the dim side of the ring. This observable feature correlates with spin of the black hole [4].

4.3. Physics Inference Model

The four features from the previous analysis create an information bottleneck, where plasma features identified as important by astrophysicists are distilled from a forecasted simulation. This physics-informed inductive bias enables more data-efficient and robust parameter estimation. The final stage of BHCAST's pipeline is a classification model that takes a set of plasma features as input, and outputs a category for the spin parameter a_* and the inclination parameter i. To train the model, we generate a dataset with plasma features computed on slices of the GRMHD training movies combined with features extracted from forecasts.

Instead of a deep neural network, we choose a popular gradient-boosting decision tree framework, XGBoost, to perform the feature classification task. The key consideration here is the quantitative feature importance scores and predictive confidence scores from XGBoost, which offer interpretable parameter inference results [8]. Our experiments identify pattern speed as most important for inclination classification and asymmetry for spin classification. Full importance score metrics are listed in Appendix B. In addition to interpretability, gradient boosting decision trees are well suited for handling heterogeneous tabular data and are invariant to the scale of different features [39].

5. Forecasting Sgr A*

We empirically study our proposed framework on the Sgr A* dataset through a three-part evaluation:

1. Most importantly, we demonstrate that our dynamics surrogate model super-resolves a blurry input image and performs long-term stable forecast.
2. From the forecast, we extract plasma features and show that they are consistent with the ground truth.
3. Finally, we infer black hole parameters and demonstrate the robustness of BHCAST to the input image resolution.

Note that BHCAST accomplishes all these tasks within a single inference pass, whereas each baseline handles a single task and must be trained independently.

5.1. Super-Resolution and Long-Term Forecasting

This subsection focuses on results for super-resolving a blurry input and long-term autoregressive forecasting.

Baseline We compare to two alternative forecasting approaches, one deep-learning and one non-learning baseline. While our model simultaneously super-resolves and evolves dynamics, prior research has developed tools that specialize in either super-resolution or forecasting. Thus, our baselines decouple the two tasks. The **learning baseline** first uses a pretrained enhanced deep super-resolution network (EDSR), finetuned on GRMHD data, to super-resolve the blurry input image; then, a convolutional LSTM (ConvLSTM) trained on unblurred simulations uses the output from EDSR to forecast dynamics [23, 37, 51]. The non-learning baseline consists of a Wiener deconvolution module followed by an optical flow model to evolve the image [20, 61]. Given a test frame, we allow access to the ground truth mean optical flow for forecasting. Thus, the non-learning pipeline is an **oracle baseline**.

Super-Resolution Conventional super-resolution methods operate in a one-shot manner: given a blurry image, the model directly predicts a sharper version in a single step. In contrast, our dynamics-based approach sharpens the image through time: the first predicted frame is noticeably clearer than the input, and each subsequent autoregressive forecast becomes progressively sharper. This behavior arises because the GRMHD simulations form a global attractor – a manifold of physically-plausible states (frames) in the training data. A blurry input, lacking high-frequency detail, lies

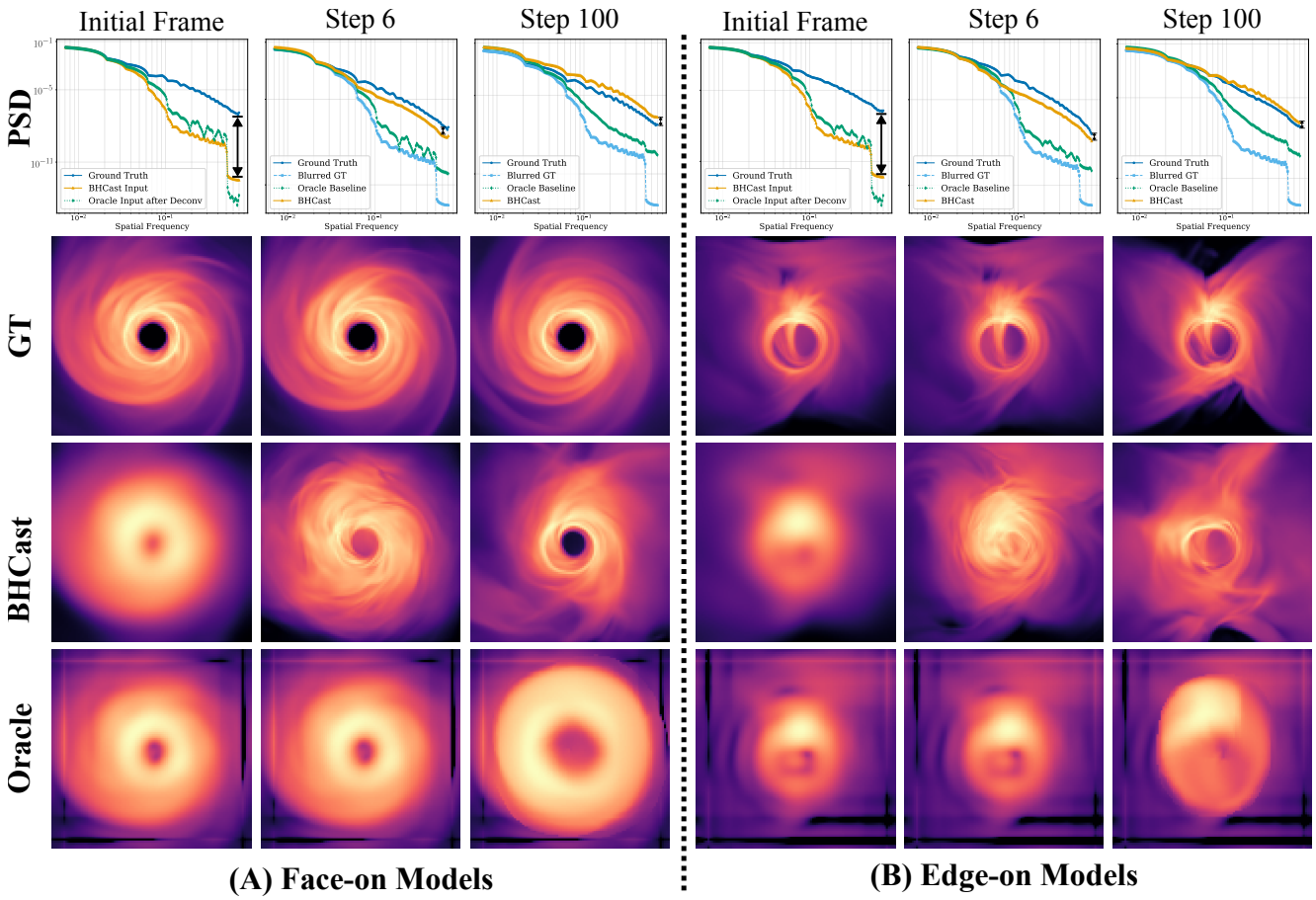


Figure 4. **Super-Resolution Evaluation**: Power Spectral Density (PSD) and log-scale visualizations of the input, prediction after 6 steps (30 GMc^{-3}), and prediction after 100 steps (500 GMc^{-3}) for (A) face-on GRMHD and (B) edge-on GRMHD. At input, BHCAST lacks high-frequency details but recovers them by step 6 to match the ground truth PSD. Its forecasts also visually converge to the ground truth. The oracle optical flow baseline starts with the deconvolution result but shows limited super-resolution. The learning-based baseline is omitted due to divergence after a few steps.

off this manifold. The trained dynamics model projects the input back onto the manifold, effectively *pulling* forecasts into the space of physically realistic states and restoring high-frequency detail. Subsequent predictions remain stable and physically consistent. To evaluate super-resolution, we adopt the power spectral density (PSD) as a measure of spatial detail [48]. A good super-resolved forecast should match the ground-truth PSD. As shown in Fig. 4, averaged across all test cases, BHCAST begins from a low-frequency, blurry input, unlike baselines that super-resolve before forecasting, yet after six forecast steps its PSD recovers the missing high-frequency content. Fig. 4 illustrates the PSD result with two forecast test cases, one for face-on GRMHD models (top-down view) and one for edge-on (side view). In both cases, BHCAST super-resolves the dominant ring by step 6 and maintains spiral arm features that resemble the ground truth until the end of the forecast.

Forecast Fidelity Fig. 5 shows the LPIPS over 100 forecast steps, averaged over test inputs. The learning baseline deteriorates rapidly, while BHCAST achieves the lowest LPIPS and preserves dynamics throughout the roll-out.

5.2. Plasma Feature Analysis

This subsection evaluates the accuracy of plasma features extracted from BHCAST's forecast.

Baseline As a point of comparison, we consider a supervised regression model that estimates the features directly from the input image, bypassing the cylinder-plots analysis. We train a ResNet50 model similar in parameter count to our U-Net surrogate on (image, feature) pairs, where features are computed from the training set [25]. Since we compute four distinct features, we treat them as individual tasks and train four separate ResNet models, while BHCAST extracts all features from a single forecasted movie.

As a powerful feature extractor, the ResNet baseline

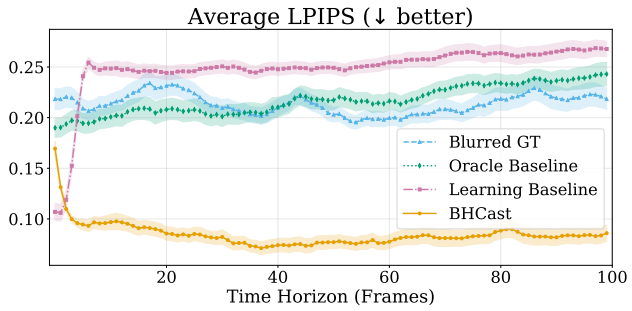


Figure 5. **Forecasting Fidelity Evaluation.** Perceptual similarity (LPIPS; lower is better) between forecasts and the unblurred ground-truth simulation. BHCAST's forecast remains visually close to the ground truth over long horizons, while baseline forecasts are on par with the EHT-resolution blurred input.

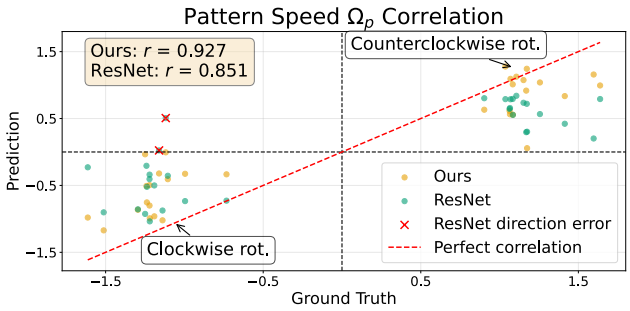


Figure 6. **Pattern Speed Correlation**. Extracted pattern speed from a 60-frame forecast shows a very strong correlation of 0.927 with the ground truth values. In addition, BHCAST identifies separate clusters for clockwise and counter-clockwise rotation, showing significantly less bias than the baseline when estimating counterclockwise rotation.

Table 1. **Mean Absolute Error ± Standard Error (↓) of extracted plasma features, averaged across all test cases.** Our BHCast model is compared against a ResNet baseline.

Plasma Feature	BHCAST	ResNet Baseline
Pattern Speed (Ω_p)	**0.46 ± 0.05**	0.64 ± 0.07
Pitch Angle (Φ)	**0.13 ± 0.01**	0.14 ± 0.02
Asymmetry	0.30 ± 0.03	**0.23 ± 0.02**
Rotation Curve Slope	**0.24 ± 0.03**	0.25 ± 0.03

achieves almost perfect mean absolute error (MAE) on the validation set for each regression task. However, when tested on blurry images, the distribution shift leads to increased errors. Tab. 1 compares the MAE with standard error (SE) of BHCAST to the ResNet baselines. Despite accumulating error inherent to autoregressive prediction, BHCAST extracts pattern speed Ω_p significantly better, while remaining on par with direct estimation for other features.

In addition to reporting the absolute error, Fig. 6 demonstrates strong correlation of 0.927 between BHCAST's extracted and ground truth pattern speeds. Our estimates of counter-clockwise rotation speeds are less biased than the baseline. For the remaining plasma features the correlations are 0.758 for pitch angle, 0.626 for asymmetry, and 0.610 for rotation curve slope. Correlation plots for these additional features are provided in Appendix B.

5.3. Black Hole Parameter Inference

This subsection presents the parameter inference accuracies and robustness to shifts in the input image distribution.

Baseline Since our GRMHD data only covers **discrete values of spin and inclination**, a convolutional neural network can directly predict the class from an image. We train two additional ResNet50 models, one for inclination and one for spin, until convergence. There are two classes for spin prediction: prograde ($a_* > 0$) and retrograde ($a_* < 0$), and four classes for inclination prediction: negative face-on, negative edge-on, positive edge-on, positive face-on.

Table 2. **Classification accuracy of black hole parameters, comparing BHCAST to a ResNet baseline.** The 20 μas (EHT-like) resolution is the baseline. The 25 μas and 30 μas rows show the performance degradation (or stability) as blurring increases, with differences (Δ) relative to the baseline.

Blurring Level	Model	Inclination Accuracy	Spin Accuracy
20 μas (Baseline)	**BHCAST**	**56.41%**	**69.22%**
	ResNet	47.19%	67.66%
25 μas	**BHCAST**	**56.72%** (+0.31)	**71.09%** (+1.87)
	ResNet	31.41% (-15.78)	54.53% (-13.13)
30 μas	**BHCAST**	**53.44%** (-2.97)	**65.78%** (-3.44)
	ResNet	25.47% (-21.72)	44.37% (-23.29)

At test time, we vary the blurring kernel to differ from the standard EHT-resolution of 20 μas to include 25 μas and 30 μas options for testing robustness to distribution shift. Evaluated on 640 samples, Tab. 2 demonstrates the superior accuracy of BHCAST with the standard 20μas EHT-resolution blurring. Moreover, changing the blurring kernel leads to massive degradation of the supervised baseline. In contrast, BHCAST is robust to different blurring kernels, due to effective super-resolution of the dynamics model and the accuracy of plasma feature estimation. We include additional robustness studies in Appendix B.

Uncertainty Quantification via Bootstrapping We perform bootstrapping by training an ensemble of 100 models on random 80% portions of the training set of plasma features. On the held-out validation set, we measure the ensemble's *aleatoric uncertainty* via average score entropy and *epistemic uncertainty* via average variance [27, 28]. In Tab. 3, the extremely-low epistemic uncertainties for both spin and inclination prediction indicate that the ensemble unanimously agrees on predictions. The errors stem from a small portion of data outliers as aleatoric uncertainty.

Dataset and Experiment Details Our GRMHD dataset consists 32 Sgr A* movies, each with a temporal window of 1,000 simulation frames with resolution 100×100 pixels. We partition the movies into 800/100/100 frames for training/validation/test sets respectively. For dynamics forecasting, a U-Net is trained on consecutive GRMHD frames from the training set, totaling 25,000 frame pair samples. For parameter inference, an XGBoost model is trained on plasma features computed on consecutive 60-frame slices from the training set and 60-frame forecasts from the trained U-Net, and the source GRMHD movie spin and inclination are used as labels. Over 30,000 samples of (plasma features, black hole label) data are generated for training. During testing, input frames are blurred to EHT resolution and two frames apart (10 GMc^{-3}) within the test set. The time horizon for test-time forecast is 60 frames (300 GMc^{-3}), such that we balance having sufficient evaluation samples and a significant length for accurate plasma features. For hyperparameters and model specifications, refer to Appendix A.

6. Forecasting M87*

In this section, we test the generalization of BHCAST by applying it to a new black hole system, M87*. Since M87* GRMHD data is very limited compared to Sgr A*, it is challenging to train a standalone dynamics model for M87*.

6.1. M87* Parameter Estimation

Previous VLBI measurements have estimated the inclination angle of M87* as either 17°or 163° [60]. The ambiguity between the two options remains due to uncertainty as to whether the accretion disk angular momentum is pointed towards or away from Earth. Given a blurry test M87* GRMHD image, we leverage an important heuristic that pattern speed has the same sign as $\cos(\text{inclination})$ to constrain this value [9]. We produce a forecast from the input image and compute the pattern speed to check its sign. We classify input images with positive predicted pattern speeds to 17°and negatives to 163°. On 168 forecasts, BHCAST achieves **78.6%** accuracy on negative samples and **58.3%** on positive samples without any training on M87* data.

Table 3. **An ensemble of XGBoost bootstrapped models achieves high accuracy with low epistemic uncertainty.** This demonstrates that the extracted plasma features are effective and lead to stable, unanimous predictions.

Metric	Spin Model	Inclination Model
Validation Accuracy	0.94	0.87
Aleatoric Uncertainty	$0.15(\in [0,1])$	$0.42(\in [0,2])$
Epistemic Uncertainty	**0.003**$(\in [0,1])$	**0.004**$(\in [0,1])$
Mean Confidence	0.96 ± 0.10	0.88 ± 0.15

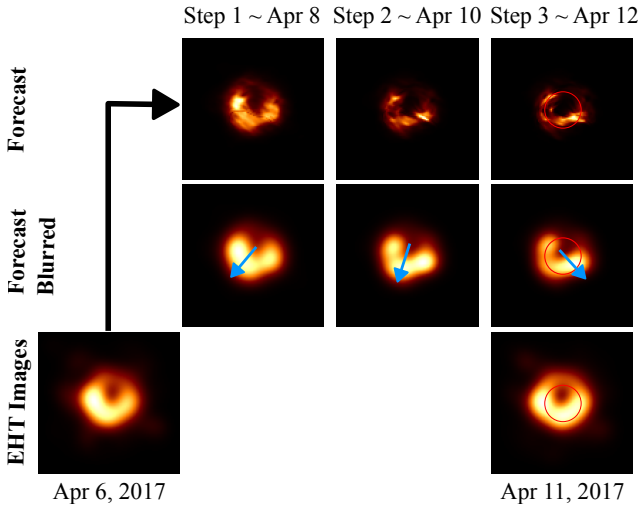


Figure 7. **Extrapolation on EHT M87* image**. We use the April 6 EHT image as input and validate our forecasting ability by comparing the blurred forecast after three autoregressive steps with the April 11 EHT image. BHCAST successfully resolves the correct ring structure (red circle) and predicts a counterclockwise rotation, consistent with the EHT reconstructions.

6.2. Testing on Real M87* Images

Although BHCAST was trained only on simulations and not on EHT reconstructions, we evaluate it on real observational data: the EHT images of M87*. The April 2017 EHT campaign captured M87* over multiple days; the April 6 and April 11 reconstructions are separated by approximately 15 GMc^{-3}, corresponding to 3 steps of our dynamics forecast model. Fig. 7 shows our forecast result resolving a stable ring structure with the correct radius. Moreover, our model predicts a counterclockwise brightness shift along the ring, consistent with the observed April 11 EHT image. Additionally, we achieve 68.9% accuracy in rotation prediction on the augmented test set of M87* images in Tab. 10.

7. Conclusion and Discussion

We introduced BHCAST, a framework that forecasts black hole dynamics from a single, blurry image. Using a physics-informed multi-scale loss, our dynamics surrogate model produces both super-resolved and stable predictions over long temporal horizons. From these forecasts, we extract physically meaningful plasma features, and use them to infer key properties of the black hole system. BHCAST therefore enables dynamical analysis even from highly blurred EHT images. Looking ahead, we plan to extend BHCAST's inference capabilities to the multi-day M87* movie campaign. By recasting a traditionally static inverse problem into a modular task of stable forecasting and physical inference, BHCAST suggests a new paradigm for scientific imaging, where dynamics are not just a byproduct of observation, but a foundational tool for discovery.

Acknowledgment

We thank Rohan Dahale for assistance with plasma feature computation and the PI-vision group/EcoSys group at University of Toronto for useful feedback on the paper. We thank Kamyar Azizzadenesheli for his important role in guiding the project. We thank Charles Gammie from UIUC for providing crucial data used in this work.

RT and GP are supported by the Canada Foundation for Innovation JELF grant, NSERC Discovery Grant, Google Scholar Research Award, VMware Early Career Faculty Grant/Award, Ontario Early Researcher Award, and the Vector CIFAR AI Chair award. NC is supported by the NASA Future Investigators in NASA Earth and Space Science and Technology (FINESST) program. This material is based upon work supported by the National Aeronautics and Space Administration under Grant No. 80NSSC24K1475 issued through the Science Mission Directorate. AS and AL are supported by the Natural Sciences and Engineering Research Council of Canada (NSERC). This work was supported by the Ontario Research Fund – Research Excellence under Project Number RE012-045.

This work was further supported by NSF grants AST 17-16327 (horizon), OISE 17-43747, and AST 20-34306. This research used resources of the Oak Ridge Leadership Computing Facility at the Oak Ridge National Laboratory, which is supported by the Office of Science of the U.S. Department of Energy under Contract No. DE-AC05-00OR22725. This research used resources of the Argonne Leadership Computing Facility, which is a DOE Office of Science User Facility supported under Contract DE-AC02-06CH11357. This research was done using services provided by the OSG Consortium, which is supported by the National Science Foundation awards #2030508 and #1836650. This research is part of the Delta research computing project, which is supported by the National Science Foundation (award OCI 2005572), and the State of Illinois. Delta is a joint effort of the University of Illinois at Urbana-Champaign and its National Center for Supercomputing Applications.

References

[1] Kazunori Akiyama, Antxon Alberdi, Walter Alef, Juan Carlos Algaba, Richard Anantua, Keiichi Asada, Rebecca Azulay, Uwe Bach, Anne-Kathrin Baczko, David Ball, et al. First sagittarius a* event horizon telescope results. v. testing astrophysical models of the galactic center black hole. *The Astrophysical Journal Letters*, 930(2):L16, 2022.

[2] K Akiyama et al. The event horizon telescope collaboration, first m87 event horizon telescope results. iii. *Data processing and calibration, Astrophys. J*, 875:L3, 2019.

[3] Michi Bauböck, Nicholas S. Conroy, Vedant Dhruv, Daeyoung Lee, Chi-Kwan Chan, Abhishek V. Joshi, Ben S. Prather, and Charles F. Gammie. Spiral Feature Pitch Angles from Event Horizon Telescope Movies. *The Astrophysical Journal*, 2025. in preparation.

[4] Vadim Bernshteyn, Nicholas S. Conroy, and Michi et al. Bauböck. Ring Asymmetry and Spin in M87*. *arXiv e-prints*, art. arXiv:2601.00394, 2026.

[5] G. S. Bisnovatyi-Kogan and A. A. Ruzmaikin. The Accretion of Matter by a Collapsing Star in the Presence of a Magnetic Field. *Astrophysics and Space Science*, 28(1):45–59, 1974.

[6] Peter J Burt and Edward H Adelson. The laplacian pyramid as a compact image code. In *Readings in computer vision*, pages 671–679. Elsevier, 1987.

[7] Ricky TQ Chen, Yulia Rubanova, Jesse Bettencourt, and David K Duvenaud. Neural ordinary differential equations. *Advances in neural information processing systems*, 31, 2018.

[8] Tianqi Chen and Carlos Guestrin. Xgboost: A scalable tree boosting system. In *Proceedings of the 22nd acm sigkdd international conference on knowledge discovery and data mining*, pages 785–794, 2016.

[9] Nicholas S Conroy, Michi Bauböck, Vedant Dhruv, Daeyoung Lee, Avery E Broderick, Chi-kwan Chan, Boris Georgiev, Abhishek V Joshi, Ben Prather, and Charles F Gammie. Rotation in event horizon telescope movies. *The Astrophysical Journal*, 951(1):46, 2023.

[10] Nicholas S Conroy, Michi Bauböck, Vedant Dhruv, Daeyoung Lee, Chi-kwan Chan, Abhishek V Joshi, Ben Prather, and Charles F Gammie. Event horizon telescope pattern speeds in the visibility domain. *arXiv preprint arXiv:2510.08848*, 2025.

[11] Vedant Dhruv, Ben Prather, George N. Wong, and Charles F. Gammie. A Survey of General Relativistic Magnetohydrodynamic Models for Black Hole Accretion Systems. *The Astrophysical Journal Supplement Series*, 277(1):16, 2025.

[12] Anurag Dutta, John Harshith, A Ramamoorthy, and K Lakshmanan. Attractor inspired deep learning for modelling chaotic systems. *Human-Centric Intelligent Systems*, 3(4): 461–472, 2023.

[13] J-P Eckmann and David Ruelle. Ergodic theory of chaos and strange attractors. *Reviews of modern physics*, 57(3):617, 1985.

[14] Zachariah B Etienne, Vasileios Paschalidis, Roland Haas, Philipp Mösta, and Stuart L Shapiro. Illinoisgrmhd: an open-source, user-friendly grmhd code for dynamical spacetimes. *Classical and Quantum Gravity*, 32(17):175009, 2015.

[15] Event Horizon Telescope Collaboration, K. Akiyama, A. Alberdi, W. Alef, and et al. First m87 event horizon telescope results. i. the shadow of the supermassive black hole. *Astrophysical Journal Letters*, 875(1):L1, 2019.

[16] Event Horizon Telescope Collaboration, K. Akiyama, A. Alberdi, W. Alef, and et al. First sagittarius a* event horizon telescope results. i. the shadow of the supermassive black hole in the center of the milky way. *Astrophysical Journal Letters*, 930(2):L12, 2022.

[17] Event Horizon Telescope Collaboration, K. Akiyama, A. Alberdi, W. Alef, and et al. First sagittarius a* event horizon telescope results. iv. variability, morphology, and mitigation strategies. *Astrophysical Journal Letters*, 930(2):L15, 2022.

[18] Event Horizon Telescope Collaboration, K. Akiyama, and et al. A persistent shadow of the supermassive black hole in m87. *Astrophysical Journal Letters*, 957(1):L20, 2023.

[19] Joseph Farah, Jordy Davelaar, Daniel Palumbo, Michael Johnson, and Jonathan Delgado. Machine and deep learning–driven angular momentum inference from bhex observations of the n= 1 photon ring. *The Astrophysical Journal*, 983(2):185, 2025.

[20] Gunnar Farnebäck. Two-frame motion estimation based on polynomial expansion. In *Scandinavian conference on Image analysis*, pages 363–370. Springer, 2003.

[21] Golnaz Ghiasi and Charless C Fowlkes. Laplacian pyramid reconstruction and refinement for semantic segmentation. In *European conference on computer vision*, pages 519–534. Springer, 2016.

[22] Daniel Glasner, Shai Bagon, and Michal Irani. Super-resolution from a single image. In *2009 IEEE 12th international conference on computer vision*, pages 349–356. IEEE, 2009.

[23] Gabriel Gouvine. Super-resolution networks for pytorch. `https://github.com/Coloquinte/torchSR`, 2021.

[24] EK Grassberg, VS Imshennik, and DK Nadyozhin. On the theory of the light curves of supernovae. *Astrophysics and Space Science*, 10(1):28–51, 1971.

[25] Kaiming He, Xiangyu Zhang, Shaoqing Ren, and Jian Sun. Deep residual learning for image recognition. In *Proceedings of the IEEE conference on computer vision and pattern recognition*, pages 770–778, 2016.

[26] Jonathan Ho, Ajay Jain, and Pieter Abbeel. Denoising diffusion probabilistic models. *Advances in neural information processing systems*, 33:6840–6851, 2020.

[27] Eduard Hofer, Martina Kloos, Bernard Krzykacz-Hausmann, Jörg Peschke, and Martin Woltereck. An approximate epistemic uncertainty analysis approach in the presence of epistemic and aleatory uncertainties. *Reliability Engineering & System Safety*, 77(3):229–238, 2002.

[28] Neil Houlsby, Ferenc Huszár, Zoubin Ghahramani, and Máté Lengyel. Bayesian active learning for classification and preference learning. *arXiv preprint arXiv:1112.5745*, 2011.

[29] Igor V. Igumenshchev, Ramesh Narayan, and Marek A. Abramowicz. Three-dimensional Magnetohydrodynamic Simulations of Radiatively Inefficient Accretion Flows. *The Astrophysical Journal*, 592(2):1042–1059, 2003.

[30] S. Issaoun, M. D. Johnson, L. Blackburn, A. Broderick, P. Tiede, M. Wielgus, S. S. Doeleman, H. Falcke, K. Akiyama, G. C. Bower, C. D. Brinkerink, A. Chael, I. Cho, J. L. Gómez, A. Hernández-Gómez, D. Hughes, M. Kino, T. P. Krichbaum, E. Liuzzo, L. Loinard, S. Markoff, D. P. Marrone, Y. Mizuno, J. M. Moran, Y. Pidopryhora, E. Ros, K. Rygl, Z.-Q. Shen, and J. Wagner. Persistent non-gaussian structure in the image of sagittarius a* at 86 ghz. *The Astrophysical Journal*, 915(2):99, 2021.

[31] Michael D. Johnson, Ramesh Narayan, Dimitrios Psaltis, Lindy Blackburn, Yuri Y. Kovalev, Carl R. Gwinn, Guang-Yao Zhao, Geoffrey C. Bower, James M. Moran, Motoki Kino, Michael Kramer, Kazunori Akiyama, Jason Dexter, Avery E. Broderick, and Lorenzo Sironi. The scattering and intrinsic structure of sagittarius a* at radio wavelengths. *The Astrophysical Journal*, 865(2):104, 2018.

[32] George Em Karniadakis, Ioannis G Kevrekidis, Lu Lu, Paris Perdikaris, Sifan Wang, and Liu Yang. Physics-informed machine learning. *Nature Reviews Physics*, 3(6):422–440, 2021.

[33] Anat Levin, Yair Weiss, Fredo Durand, and William T Freeman. Understanding and evaluating blind deconvolution algorithms. In *2009 IEEE conference on computer vision and pattern recognition*, pages 1964–1971. IEEE, 2009.

[34] Aviad Levis, Daeyoung Lee, Joel A Tropp, Charles F Gammie, and Katherine L Bouman. Inference of black hole fluid-dynamics from sparse interferometric measurements. In *Proceedings of the IEEE/CVF International Conference on Computer Vision*, pages 2340–2349, 2021.

[35] Zongyi Li, Nikola Kovachki, Kamyar Azizzadenesheli, Burigede Liu, Kaushik Bhattacharya, Andrew Stuart, and Anima Anandkumar. Fourier neural operator for parametric partial differential equations. *arXiv preprint arXiv:2010.08895*, 2020.

[36] Zongyi Li, Miguel Liu-Schiaffini, Nikola Kovachki, Burigede Liu, Kamyar Azizzadenesheli, Kaushik Bhattacharya, Andrew Stuart, and Anima Anandkumar. Learning dissipative dynamics in chaotic systems. *arXiv preprint arXiv:2106.06898*, 2021.

[37] Bee Lim, Sanghyun Son, Heewon Kim, Seungjun Nah, and Kyoung Mu Lee. Enhanced deep residual networks for single image super-resolution. In *Proceedings of the IEEE conference on computer vision and pattern recognition workshops*, pages 136–144, 2017.

[38] Scott M Lundberg and Su-In Lee. A unified approach to interpreting model predictions. *Advances in neural information processing systems*, 30, 2017.

[39] Duncan McElfresh, Sujay Khandagale, Jonathan Valverde, Vishak Prasad C, Ganesh Ramakrishnan, Micah Goldblum, and Colin White. When do neural nets outperform boosted trees on tabular data? *Advances in Neural Information Processing Systems*, 36:76336–76369, 2023.

[40] Tomer Michaeli and Michal Irani. Nonparametric blind super-resolution. In *Proceedings of the IEEE international conference on computer vision*, pages 945–952, 2013.

[41] John Milnor. On the concept of attractor. *Communications in Mathematical Physics*, 99(2):177–195, 1985.

[42] Monika Moscibrodzka and Charles F. Gammie. ipole - semi-analytic scheme for relativistic polarized radiative transport, 2017.

[43] Ramesh Narayan, Igor V. Igumenshchev, and Marek A. Abramowicz. Magnetically Arrested Disk: an Energetically Efficient Accretion Flow. *Publications of the Astronomical Society of Japan*, 55(6):L69–L72, 2003.

[44] Oliver Porth, Koushik Chatterjee, Ramesh Narayan, and Charles F. Gammie et al. The event horizon general relativistic magnetohydrodynamic code comparison project. *The Astrophysical Journal Supplement Series*, 243(2):26, 2019.

[45] Ben S. Prather. KHARMA: Flexible, Portable Performance for GRMHD. *arXiv e-prints*, art. arXiv:2408.01361, 2024.

[46] Maziar Raissi, Paris Perdikaris, and George E Karniadakis. Physics-informed neural networks: A deep learning framework for solving forward and inverse problems involving nonlinear partial differential equations. *Journal of Computational physics*, 378:686–707, 2019.

[47] Angelo Ricarte, Daniel C. M. Palumbo, Ramesh Narayan, Freek Roelofs, and Razieh Emami. Observational signatures of frame dragging in strong gravity. *The Astrophysical Journal Letters*, 941(1):L12, 2022.

[48] Dirk Robinson and Peyman Milanfar. Statistical performance analysis of super-resolution. *IEEE Transactions on Image Processing*, 15(6):1413–1428, 2006.

[49] Olaf Ronneberger, Philipp Fischer, and Thomas Brox. U-net: Convolutional networks for biomedical image segmentation. In *International Conference on Medical image computing and computer-assisted intervention*, pages 234–241. Springer, 2015.

[50] Jeremy D Schnittman, Julian H Krolik, and John F Hawley. Light curves from an mhd simulation of a black hole accretion disk. *The Astrophysical Journal*, 651(2):1031, 2006.

[51] Xingjian Shi, Zhourong Chen, Hao Wang, Dit-Yan Yeung, Wai-Kin Wong, and Wang-chun Woo. Convolutional lstm network: A machine learning approach for precipitation nowcasting. *Advances in neural information processing systems*, 28, 2015.

[52] Kiwhan Song, Boyuan Chen, Max Simchowitz, Yilun Du, Russ Tedrake, and Vincent Sitzmann. History-guided video diffusion. *arXiv preprint arXiv:2502.06764*, 2025.

[53] Alexander Tchekhovskoy, Ramesh Narayan, and Jonathan C. McKinney. Efficient generation of jets from magnetically arrested accretion on a rapidly spinning black hole. *Monthly Notices of the Royal Astronomical Society: Letters*, 418(1): L79–L83, 2011.

[54] The Event Horizon Telescope Collaboration, Kazunori Akiyama, Antxon Alberdi, Walter Alef, and Keiichi Asada et. al. First m87 event horizon telescope results. v. physical origin of the asymmetric ring. *The Astrophysical Journal Letters*, 875(1):L5, 2019.

[55] The Event Horizon Telescope Collaboration, Kazunori Akiyama, Antxon Alberdi, Walter Alef, Juan Carlos Algaba, Richard Anantua, and Asada et al. First sagittarius a* event horizon telescope results. iii. imaging of the galactic center supermassive black hole. *The Astrophysical Journal Letters*, 930(2):L14, 2022.

[56] The Event Horizon Telescope Collaboration, Kazunori Akiyama, Antxon Alberdi, and Walter Alef et al. First sagittarius a* event horizon telescope results. v. testing astrophysical models of the galactic center black hole. *The Astrophysical Journal Letters*, 930(2):L16, 2022.

[57] Nithyanandan Thyagarajan, Lucas Hoefs, and O Ivy Wong. Interferometric image reconstruction using closure invariants and machine learning. *RAS Techniques and Instruments*, 3 (1):437–452, 2024.

[58] Jeffrey Van der Gucht, Jordy Davelaar, Luc Hendriks, Oliver Porth, Hector Olivares, Yosuke Mizuno, Christian M Fromm, and Heino Falcke. Deep horizon: A machine learning network that recovers accreting black hole parameters. *Astronomy & Astrophysics*, 636:A94, 2020.

[59] Ashish Vaswani, Noam Shazeer, Niki Parmar, Jakob Uszkoreit, Llion Jones, Aidan N Gomez, Łukasz Kaiser, and Illia Polosukhin. Attention is all you need. *Advances in neural information processing systems*, 30, 2017.

[60] R Craig Walker, Philip E Hardee, Frederick B Davies, Chun Ly, and William Junor. The structure and dynamics of the subparsec jet in m87 based on 50 vlba observations over 17 years at 43 ghz. *The Astrophysical Journal*, 855(2):128, 2018.

[61] Norbert Wiener. *Extrapolation, interpolation, and smoothing of stationary time series*. The MIT press, 1964.

[62] Joshua N Winn, Matthew J Holman, Guillermo Torres, Peter McCullough, Christopher Johns-Krull, David W Latham, Avi Shporer, Tsevi Mazeh, Enrique Garcia-Melendo, Cindy Foote, et al. The transit light curve project. ix. evidence for a smaller radius of the exoplanet xo-3b. *The Astrophysical Journal*, 683(2):1076, 2008.

[63] George N. Wong, Ben S. Prather, Vedant Dhruv, Benjamin R. Ryan, Monika Mościbrodzka, Chi-kwan Chan, Abhishek V. Joshi, Ricardo Yarza, Angelo Ricarte, Hotaka Shiokawa, Joshua C. Dolence, Scott C. Noble, Jonathan C. McKinney, and Charles F. Gammie. PATOKA: Simulating Electromagnetic Observables of Black Hole Accretion. *The Astrophysical Journal Supplement Series*, 259(2):64, 2022.

[64] AI Yfantis, S Zhao, R Gold, M Mościbrodzka, and AE Broderick. Testing bayesian inference of grmhd model parameters from vlbi data. *Monthly Notices of the Royal Astronomical Society*, 535(4):3181–3197, 2024.

[65] Bingliang Zhang, Zihui Wu, Berthy T Feng, Yang Song, Yisong Yue, and Katherine L Bouman. Step: A general and scalable framework for solving video inverse problems with spatiotemporal diffusion priors. *arXiv preprint arXiv:2504.07549*, 2025.

[66] Richard Zhang, Phillip Isola, Alexei A Efros, Eli Shechtman, and Oliver Wang. The unreasonable effectiveness of deep features as a perceptual metric. In *Proceedings of the IEEE conference on computer vision and pattern recognition*, pages 586–595, 2018.

[67] Maria Zontak and Michal Irani. Internal statistics of a single natural image. In *CVPR 2011*, pages 977–984. IEEE, 2011.